INTERNATIONAL JOURNAL OF
ENERGY AND ENVIRONMENT

Volume 7, Issue 5, 2016 pp.397-416
Journal homepage: www.IJEE.IEEFoundation.org

Detached-Eddy Simulations (DES) of a complex swirl stabilized gas turbine model combustor

Ahlem Ben Sik Ali[1], Wassim Kriaa[1], Hatem Mhiri[1], Philippe Bournot[2]

[1] UTTPI, National Engineering School, Monastir, Tunisia.
[2] IUSTI, UMR CNRS 6595, 5 Rue Enrico Fermi, Technopôle de Château- Gombert, 13013 Marseille, France.

Abstract
The reacting flow in a double swirl gas turbine model combustor is studied by DES (Detached Eddy Simulation) and URANS (Unsteady Reynolds-Averaged Navier–Stokes) methods. The computational domain matches the complex laboratory configuration of a 35 kW burner, developed by the German Aerospace Center (DLR), fed with methane and characterized by a 0.65 overall equivalence ratio. The three dimensional calculations are conducted using an unstructured grid and the commercial finite-volume solver ANSYS–FLUENT. In order to evaluate their quality, the modeling results were compared with the previous experimental data. It was found that the SST-DES model reproduces better physics and shows good quantitative comparisons with the experiments. The results show that simulations using the Shear Stress Transport (SST) k-ω turbulence model over-predict the temperature compared to those using the SST-DES model and experimental data. Moreover, the SST-DES model provides much detailed information about the instantaneous flow patterns than the SST k-ω turbulence model.

Keywords: Swirling flow; CFD; DES; Gas turbine model combustor.

1. Introduction

Swirling flows are widely used in various industrial applications. Especially, the swirl is being extensively used in gas turbine combustors where it plays a predominant role in flame stabilization process. Swirling reacting flows within such complex configurations are characterized by very complicated flow patterns, due to the multiple phenomena implicated and including; vortex breakdown ,central and corner recirculation zones, precessing vortex core (PVC),...etc. The correct numerical simulation of these flows is, therefore, difficult and presents one to the most important and challenging tasks in modern Computational Fluid Dynamics (CFD) especially for the complex geometry of gas turbine combustors.

The methodologies to model turbulence in CFD range from Reynolds Averaged Navier Stokes (RANS) methods, in which the entire spectrum of turbulent motions is described by a statistical model, to Large Eddy Simulation (LES), in which only the largest local scales are resolved while the smallest are modelled. Conceptually between these extremes lies the technique of hybrid RANS/LES.

The most important advantage of RANS models is their moderate computational cost and their applicability for industrial complex configurations. In fact, numerous recent works concerned on high swirling turbulent confined combustors [1-4], indicated good agreements between the measured data and

calculated ones using the RANS turbulence models proving that the mean flow phenomena in swirling flows can be predicted accurately using RANS models. Although successful results have been obtained by RANS method, the LES is expected to be more accurate and reliable than RANS for the flows in which large-scale unsteadiness is significant [5]. In the past few years, the LES approach has been applied to the simulation of a wide range of premixed and non-premixed [6-9] swirling reacting flows in both industrial and laboratory combustors but this method still unfavourable in terms of its high demand on computational effort.

Recently, the hybrid RANS/LES have appeared as a technique that represents a good compromise between the expensive LES and less accurate RANS procedures for high-Reynolds number industrial flows and are increasingly becoming the models of choice for such applications. Compared to the LES approach the hybrid RANS/LES approaches save order of magnitudes of computing cost, since the boundary layers are RANS regions [10].

The Detached-Eddy Simulation (DES) is a hybrid technique first proposed by Spalart et al. [11] based on the Spalart–Allmaras turbulence model, for the prediction of turbulent flows at high Reynolds numbers. The original intent of the DES method was to be run in RANS mode for attached boundary layers and to switch to the LES mode in large separated (detached) flow regions. Later this technique was generalized by Strelets for applications with different underlying RANS models [12]. The DES technique was aimed primarily at external flows [13]. However, the DES turbulence model is increasingly being used as an engineering tool to predict the characteristics of a variety of complex industrial flows, namely: the injection and mixing in a scramjet combustor [14], safety related studies (jet of methane gas released into a ventilated small room) [15], the mixing characteristics of the gas–solid two-phase jet flow [16], channel flow [17], internal cooling duct [18], isothermal swirling flow [19, 20],…etc.

Nevertheless, to the best of the authors' knowledge, none have reported the swirling reacting flow within a complex gas turbine model combustor (GTMC) using the DES method. In particular, Widenhorn et al [20] conducted numerical simulations of the isothermal swirling flow within the same GTMC as that studied in this paper applying the Shear Stress Transport (SST) k-ω model, DES method, and Scale Adaptive Simulation (SAS) model and better results were obtained using the two hybrid RANS/LES approaches. The reacting flow was also studied [21, 22] using the SAS model [23] in combination with the Eddy Dissipation /Finite Rate combustion model applying a one-step global reaction mechanism for methane combustion and good agreement was found between numerical results and experimental data. For the numerical simulations the commercial CFD package ANSYS CFX 11.0 was used. The authors showed that the DES method gives good results for the cold flow; nevertheless results for the reacting flow were not presented.

We propose, in this paper to explore the feasibility of using the DES method in solving three-dimensional reacting swirling flow within a GTMC. The studied geometry corresponds to that investigated numerically by Widenhorn et al [21, 22] and experimentally in numerous works [24-30]. Numerical investigations of the flow are conducted using the URANS SST k-ω and the SST-DES turbulence models in combination with the Eddy Dissipation combustion model applying a two-step global reaction mechanism for methane combustion. The obtained numerical results are presented and compared with experimental data.

2. Geometry description

The studied GTMC represents a modified version of a practical gas turbine combustor. It was designed by the German Aerospace Center (DLR) at a laboratory-scale. Despite numerous experimental studies [24-30] focused on the DLR lab-scale GTMC, the only studies that have deal numerically with this combustor were that of Widenhorn et al. [20] and Widenhorn et al. [21-22].

As described in detail by Weigand et al. [29], the combustor is formed by three main components, namely: a plenum, an injection system, and a combustion chamber (Figure 1).

The dry air coming from the plenum, having an inner diameter of 79 mm and a height of 65 mm, passes through two radial swirlers of the injection system. The swirlers consist of 8 channels for the central swirler and 12 channels for the annular swirler (Figure 2). Then, the air penetrates to the combustion chamber from two concentric nozzles. The gas fuel is supplied to the chamber through 72 small channels (0.5 mm × 0.5 mm) forming a ring between the two air nozzles.

The combustion chamber has a square cross section of 85 mm × 85 mm and a height of 110 mm. The exit of the combustion chamber consists of an exhaust tube which has a diameter of 40 mm and a height of 50 mm.

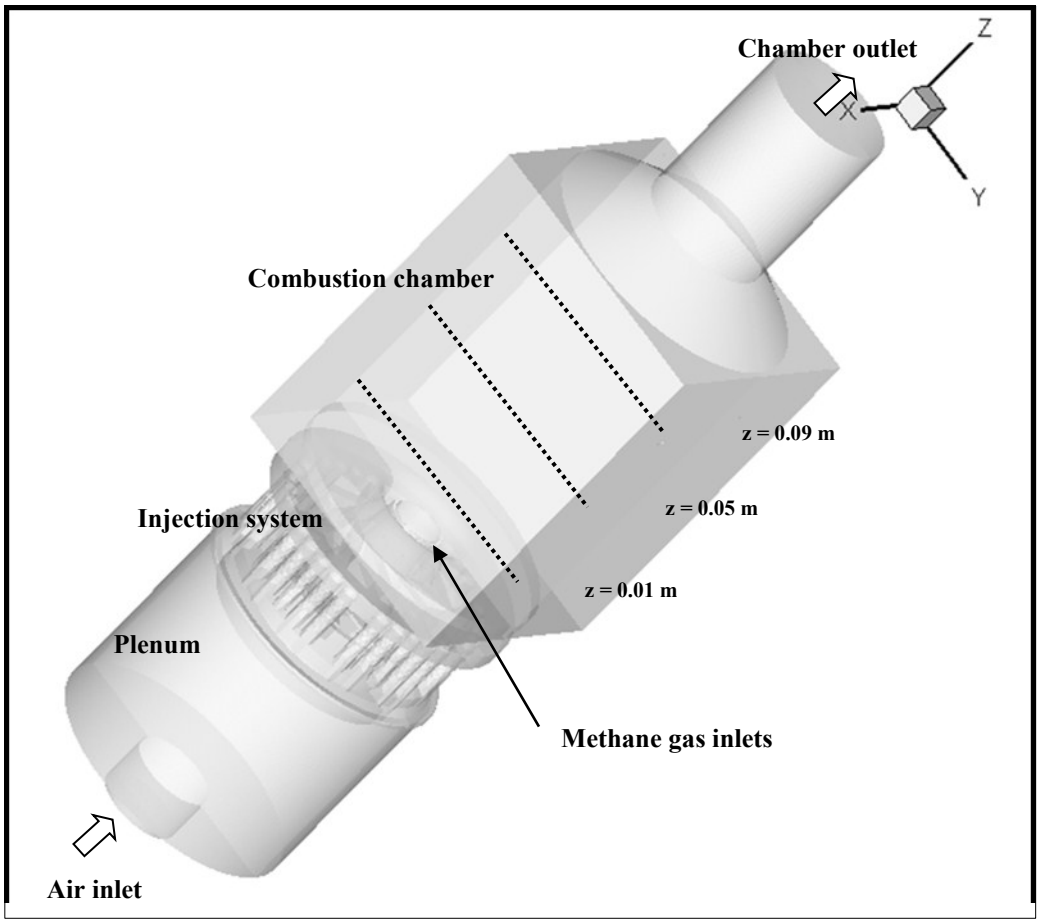

Figure 1. Computational domain of the DLR double swirl GTMC with boundary and measurement locations.

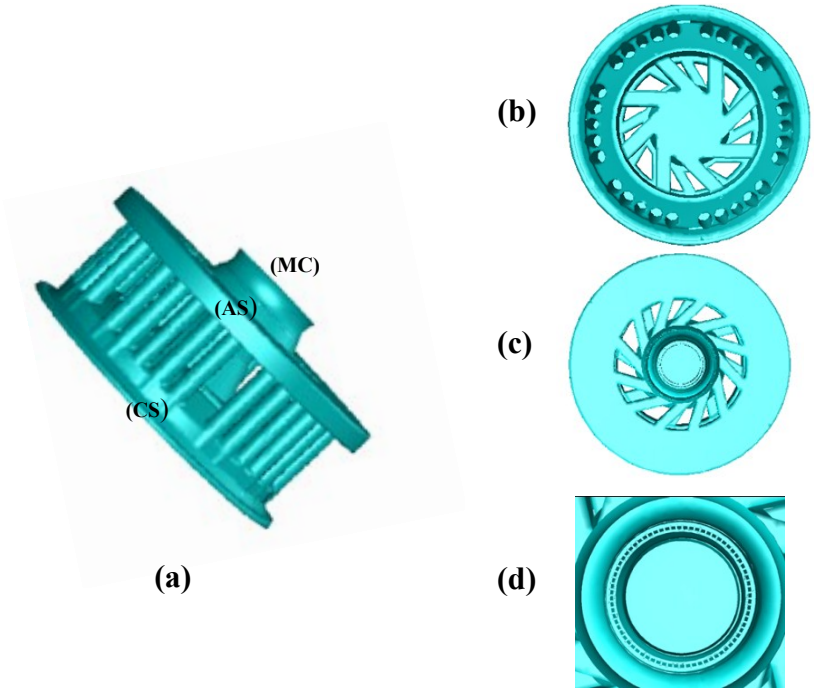

Figure 2. Injection system details: (a) The injection system, (b) The central Swirler (CS), (c) The Annular Swirler (AS), (d) Methane Channels (MC).

3. Numerical modeling

3.1 Governing equations

In these simulations, we adopted the following assumptions:
-The problem is three-dimensional and unsteady.
-An incompressible multispecies flow is considered.
-Heat capacity of each species is defined as a piecewise-polynomial function of temperature [31].
-The multispecies flow mixture is assumed to be ideal and the thermo-physical properties are calculated using the kinetic theory.
-Radiation heat transfer is neglected.
The instantaneous local balance equations are as follows:

- Mass:

$$\frac{\partial \rho}{\partial t} + \frac{\partial \rho u_j}{\partial x_j} = 0 \tag{1}$$

- Momentum (i = 1, 2, 3):

$$\frac{\partial \rho u_i}{\partial t} + \frac{\partial \rho u_j u_i}{\partial x_j} = -\frac{\partial p}{\partial x_i} + \frac{\partial \tau_{ij}}{\partial x_j} + F_i \tag{2}$$

where τ_{ij} is the viscous tensor given by:

$$\tau_{ij} = \mu\left(\frac{\partial u_i}{\partial x_j} + \frac{\partial u_j}{\partial x_i}\right) - \frac{2}{3}\mu\delta_{ij}\frac{\partial u_k}{\partial x_k} \tag{3}$$

- Species (N species with k = 1, …, N):

$$\frac{\partial \rho Y_k}{\partial t} + \frac{\partial \rho u_j Y_k}{\partial x_j} = -\frac{\partial}{\partial x_j}\left(\mathcal{J}_j^k\right) + \dot{R}_k \tag{4}$$

where $\mathcal{J}_j^k$ is the molecular diffusive flux of the species k defined as:

$$\mathcal{J}_j^k = -\rho D_k \frac{\partial Y_k}{\partial x_j} \tag{5}$$

- Total enthalpy:

$$\frac{\partial \rho h_t}{\partial t} + \frac{\partial \rho u_j h_t}{\partial x_j} = \frac{\partial p}{\partial t} + \frac{\partial}{\partial x_j}\left[\frac{\lambda}{C_p}\frac{\partial h}{\partial x_j} - \sum_{k=1}^{N} h_k \mathcal{J}_j^k + u_i \tau_{ij}\right] + u_j F_j + S_h \tag{6}$$

where ρ is the density of the fluid and u_i (i = 1, 2 and 3) are the Cartesian velocity components. F_i is the gravitational body force. Y_k is the mass fraction of the species k and D_k is the diffusion coefficient for species k in the mixture. I, h_t, and h denote respectively the unit tensor, the total non-chemical enthalpy, and the sensible enthalpy. δ_{ij} is the Kronecker symbol. λ is the thermal conductivity and C_p is the constant pressure specific heat capacity. The source term S_h is the rate of heat release in the combustion. $\dot{R}_k$ is the rate of production or consumption of the species k, determined by considering the contribution $\dot{R}_{k,r}$ of each reaction:

$$\dot{R}_k = M_k \sum_{r=1}^{N} \dot{R}_{k,r} \tag{7}$$

where M_k is the molecular weight of species k.

3.2 Turbulence models

3.2.1 The SST k-ω model

The two-equation SST k–ω turbulence model was developed by Menter [32]. This model behaves like the k–ω model [33] in near-wall regions and the well-known *k*–ε model in free flows. It also includes a modification to the definition of the turbulent viscosity, which accounts for the effect of the transport of the principal turbulent shear stress. It is noticed that the SST k–ω model includes low-Reynolds number correction in the model constants. This has the advantage that it is applicable throughout the boundary layer, if near wall meshing is sufficiently fine, and empirical wall functions are not required [33].

The transport equations for the turbulent kinetic energy *k* and the specific dissipation rate *ω* are given by equations (8) and (9).

$$\frac{\partial}{\partial t}(\rho k) + \frac{\partial}{\partial x_j}\left(\rho k \bar{u}_j\right) = \frac{\partial}{\partial x_j}\left(\left(\mu + \frac{\mu_t}{\sigma_k}\right)\frac{\partial k}{\partial x_j}\right) + P_k - Y_k \tag{8}$$

$$\frac{\partial}{\partial t}(\rho \omega) + \frac{\partial}{\partial x_j}\left(\rho \omega \bar{u}_j\right) = \frac{\partial}{\partial x_j}\left(\left(\mu + \frac{\mu_t}{\sigma_\omega}\right)\frac{\partial \omega}{\partial x_j}\right) + \frac{\rho\alpha}{\mu_t}P_k - \rho\beta\omega^2 + (1-F_1)\rho\frac{2}{\omega\sigma_{\omega,2}}\frac{\partial k}{\partial x_j}\frac{\partial \omega}{\partial x_j} \tag{9}$$

The dissipation of turbulent kinetic energy Y_k is given by:

$$Y_k = \rho\beta^* k\omega \tag{10}$$

The turbulent viscosity μ_t is computed as follows:

$$\mu_t = \frac{\rho k}{\omega}\frac{1}{max\left[\frac{1}{\alpha^*}, \frac{SF_2}{a_1\omega}\right]} \tag{11}$$

where σ_k and σ_ω are the turbulent Prandtl numbers for k and ω, respectively. S is the strain rate magnitude. The term P_k represents the production of turbulence kinetic energy. F1 and F2 are the blending functions of the SST k–ω model.

The definition of the blending functions, the production term, the coefficients (β^* and α^*), and the constants ($\sigma_{\omega,2}$ and a_1) of the SST k-ω turbulence model can be found in [34].

3.2.2 The SST-DES model

The DES is defined as a three-dimensional, unsteady numerical solution using a single turbulence model, which functions as a subgrid-scale model in regions where the grid density is fine enough for LES and as a RANS model in regions where it is not [10].

In this work, the DES approach using a modification of the shear stress transport SST k-ω turbulence model for closure is employed. The SST k-ω model is used to cover the boundary layer and switches to the LES mode in regions where the turbulent length $L_{t,SST}$ predicted by this RANS model is larger than the local grid spacing Δ defined by Δ = max (Δ x, Δ y, Δ z).

The length scale in the SST k-ω turbulence model is defined as:

$$L_{t,SST} = \frac{\sqrt{k}}{\beta^*\omega} \tag{12}$$

In the SST-DES model implementation, the length scale in the SST k-ω turbulence model is replaced by the DES length scale defined as:

$$L_{t,DES} = min\left(L_{t,SST}, L_{t,LES}\right) \tag{13}$$

where:

$$L_{t,LES} = C_{DES}\Delta \tag{14}$$

C_{DES} is a calibration constant used in the DES model and has the value of 0.61 [34].
This modification links the turbulent length scale to the local grid spacing Δ.
The term which governs the dissipation of turbulent kinetic energy in the SST k-ω RANS model is also modified according to the following expression in the DES implementation:

$$Y_k = \rho\beta^* k\omega F_{DES} \tag{15}$$

The factor F_{DES} is defined as:

$$F_{DES} = max\left(\frac{L_{t,SST}}{L_{t,LES}}, 1\right) \tag{16}$$

The DES modification is meant to switch the turbulent length scale from a RANS length scale ($\propto k^{1/2}/\omega$) to a LES length scale ($\propto \Delta$) when the grid is fine enough. When F_{DES} is larger than 1, the dissipation term Y_k increases which in turn decreases the turbulent kinetic energy k and consequently decreases the turbulent viscosity. The modeled dissipation is then reduced and a large part of the turbulence is resolved instead of being modeled.
When $L_{t,SST} > L_{t,LES}$, the model switches to a Smagorinsky type sub-grid scale model. The transition between RANS and LES is seamless in that there is a single equation with no explicit declaration of RANS versus LES zones. The formulation using a single model only leads to a discontinuity in the gradient of the length scale that enters the destruction term of the turbulence model. This discontinuity would be easily removed by rounding the min function that determines the length scale. The change in the length scale leads to a model that becomes region-dependent in nature [35].

3.3 Combustion model

Magnussen and Hjertager [36] proposed a turbulence-chemistry interaction model called the Eddy-Dissipation Model (EDM) and assumed that the rate of combustion can be determined by the rate of intermixing on a molecular scale of fuel and oxygen eddies. In this model combustion proceeds whenever turbulence is present and an ignition source is not required to initiate combustion. This is usually acceptable for non-premixed flames [34]. In highly turbulent flows corresponding to many engineering applications, the effect of chemical kinetics can be neglected. Many examples of successful using of the EDM to model turbulent combustion in industrial systems can be found in [37-40].
The reaction rates $\dot{R}_{k,r}$ in equation (7) are determined as the smaller (limiting value) of the two expressions below [35]:

$$\dot{R}_{k,r} = \vartheta'_{k,r} M_k A\rho \frac{\varepsilon}{k} \min_R \left(\frac{Y_R}{\vartheta'_{R,r} M_R}\right) \tag{17}$$

$$\dot{R}_{k,r} = \vartheta'_{k,r} M_k AB\rho \frac{\varepsilon}{k} \frac{\sum_p Y_p}{\sum_j^N \vartheta''_{j,r} M_R} \tag{18}$$

where Y_P is the mass fraction of any product species P and Y_R is the mass fraction of a particular reactant R. $\vartheta'_{k,r}$ is the stoichiometric coefficient for the reactant k in the reaction r and $\vartheta''_{j,r}$ is the stoichiometric coefficient for the product j in the reaction r.
The empirical constants *A* and *B* have respectively the values of 4 and 0.5 [34].
The chemical scheme for methane-air combustion considered in this work takes into account six species (CH4, O2, CO2, CO, H2O, and N2) and two reactions:

$CH_4+3/2O_2$—>$CO+2H2O$ (19)

$CO+1/2O_2$<—>CO_2 (20)

The first reaction is irreversible whereas the second one is reversible and leads to an equilibrium between CO and CO_2 in the burnt gases.

3.4 Boundary conditions

The boundary conditions are illustrated in Figure 1 and summarized in Table 1.

It is noticed that the geometry of interest has a rotationally periodic repeating nature by 180°. In order to reduce the computational time, the simulative domain adopted in this study was the 1/2 of the whole chamber and a periodic boundary condition was used for the side sections of the computational domain.

Table 1. The boundary conditions and flux distributions.

Boundary	Boundary condition	Flux (kg/s)	Pressure (MPa)	Temperature (K)
Combustion air inlet	Mass flow	0.01825	0.1	295
Methane gas inlets	Mass flow	0.0096 E^{-3}	0.1	295
Chamber outlet	Out flow	0.01894	-----	-----
Plenum walls	Adiabatic walls	-----	-----	-----
Combustion chamber walls	Wall	-----	-----	1050 [21]

3.5 Grid and numerical investigations

The results presented in this paper are taken from an unstructured tetrahedral mesh of approximately 3 200 000 cells, with a dimensionless wall distance of the wall-nearest grid point y+ values less than 1 in the combustion chamber . Finer grids of 3 600 000, 4 200 000, and 5 400 000 cells as well as larger grid of 1 800 000 and 2 800 000 were also tested, but mesh dependency effects were found to be small for grids counting more than 3 200 000 cells (Figure 3). The details of the used grid are illustrated in Figure 4. Considering that main core of the flow in the combustion chamber is highly turbulent a very fine grid-spacing was chosen in that zone. Larger grid spacing was chosen in the plenum zone. The minimum and maximum sizes of the cells in the combustion chamber in the used grid are on the order of Δ = 0.016 mm and Δ = 0.2 mm respectively. Those cells sizes are comparable to the Kolmogorov length scale and to integral length scale, approximately evaluated in the experiments [41] as ηk = 0.048 mm for the Kolmogorov scale and between l_0 = 1 mm and 6 mm for the integral length scale.

The time step $\Delta t = 10^{-5}$ s was chosen to be complying with the CFL (Courant–Friedrichs–Lewy) stability-condition [42]. In fact, the CFL number, representing the time step chosen, was less then unity in the entire flow domain: $CFL_{max} \leq 0.85$.

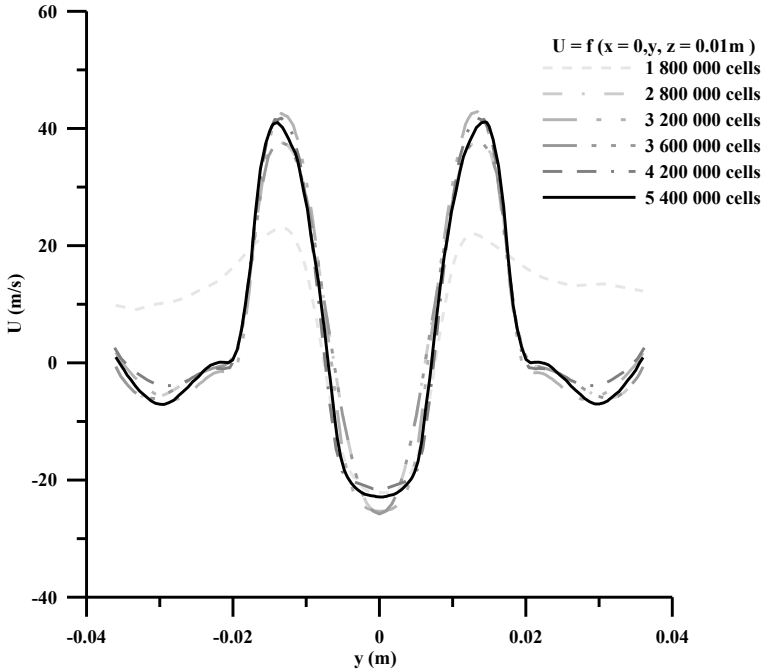

Figure 3. The average axial velocity at z = 0.01 m for the tested grids.

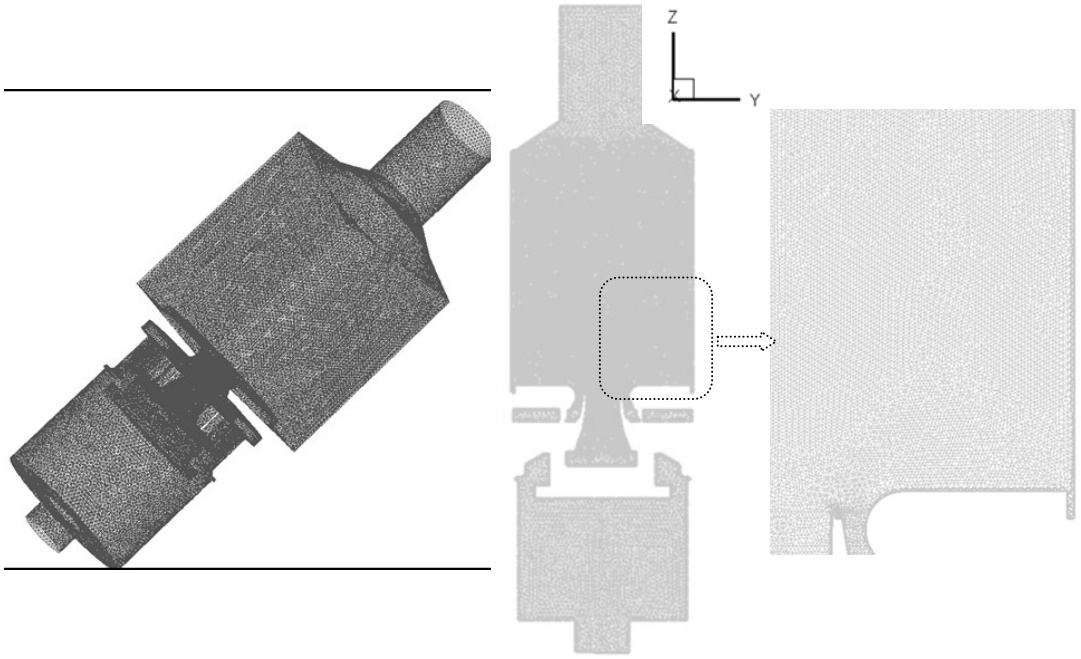

(a) (b) (c)

Figure 4. (a) Grid of the computational domain, (b) Central cross section (x = 0) and (c) Enlarged view.

The computations were carried out using 12 processors on the HP Z800 workstation. The problem is split into 12 sub-domains which are distributed into the 12 processors used. The inter-processor communication is performed with standard MPI message passing library.
The unsteady simulations were performed using the commercial CFD code ANSYS-FLUENT, which is based on finite volume discretization of the conservative governing equations. For the time discretization an implicit second order time differencing scheme is used. For the spatial discretization a bounded central difference scheme is used for the momentum equation, a second order upwind scheme for turbulence equations and a first order upwind scheme for the energy and species equations. The algorithm SIMPLE is used for the coupling of pressure and velocity.
Based on our simulations, the SST-DES model requires 15 % on average more time per iteration compared to the SST k-ω model. Furthermore, 20% more memory is needed.

4. Results and discussion

4.1 Average profiles

Numerical results obtained from the unsteady simulations using the SST-DES and the SST k-ω turbulence models were time averaged and profiles of statistical quantities were extracted on the three radial lines (z = 0.01 m , z = 0.05 m and z = 0.09 m) shown in Figure 1. The averaging time is 0.42 s corresponding to 14 combustor residence times. In the following, we compare these profiles with previous experimental data. We note that the experimental investigation of the studied configuration has been performed by the German Aerospace Center (DLR), providing complete experimental data sets useful for verification and improvement of mathematical models. Those experimental research data sets were provided to the authors by the DLR under request. Most of those experimental data were published in the experimental reference paper of Weigand et al [29].
The average axial and radial velocities are plotted in Figure 5 and Figure 6 respectively while the average tangential velocity is shown in Figure 7. Although in some of the profiles deviations can be observed, the simulation results using the two methods show a very good overall agreement with the velocity measurements. The time-averaged structure of the flow field is well reproduced by both applied methods. Especially, the proper capturing of the average velocity profiles with respect to their local maxima and minima indicates the correctly predicted rate of spreading of the swirling jets and the form, size and intensity of the flow reversal zone.
Moreover, Figure 8 shows the contours of the SST-DES and the SST k-ω models results of the negative average axial velocity marking the extension of the inner and outer recirculation zones. In fact, the outer

recirculation is due to the air stream radial expansion and the wall confinement. The inner recirculation zone results from the vortex breakdown generated by the Swirl. This large torroidal central recirculation zone plays a main role in the flame stabilization process by acting as a store for heat and chemically active species. Figure 8 puts on view that the inner recirculation zone extends up to z = 75 mm (axial direction) and reaches even into the central air nozzle for the two models which agree very well with experimental observations [29]. However, it can be clearly noticed that the SST-DES model gives a larger inner recirculation zone in comparison with the SST k-ω turbulence model.

Time averaged streamlines and axial velocity contours in the center plane of the combustor (the vertical section x = 0 m) calculated using the SST-DES and the SST k-ω models are given in Figure 9. The flow field is typical for confined swirl flames and consists of a cone-shaped stream of fresh gas entering the chamber from the injection system, an inner recirculation zone and an outer recirculation zone. Strong velocity gradients occur in the inner shear layer (ISL) between the inflow and the inner recirculation zone, and in the outer shear layer (OSL) between inflow and the outer recirculation zone. High axial velocities are found near the nozzle exit and near the exhaust duct contraction at the top. Figure 9 reveals also that central recirculation zone is highly axisymmetric, which is typical for the bubble type vortex breakdown. In fact, the axisymmetric mode of vortex breakdown or bubble breakdown [43] is characterized by a stagnation point on the swirl axis, followed by an abrupt expansion of the jet to form the envelope of a bubble of recirculating fluid. Figure 9a shows that the inner recirculation zone is formed by a pair of large axisymmetric counter rotating vortex structures. It shows also that each outer recirculation zone is formed by two small counter rotating structures. Similar results are obtained using the SST k-ω model for time averaged axial velocity field (Figure 9b).

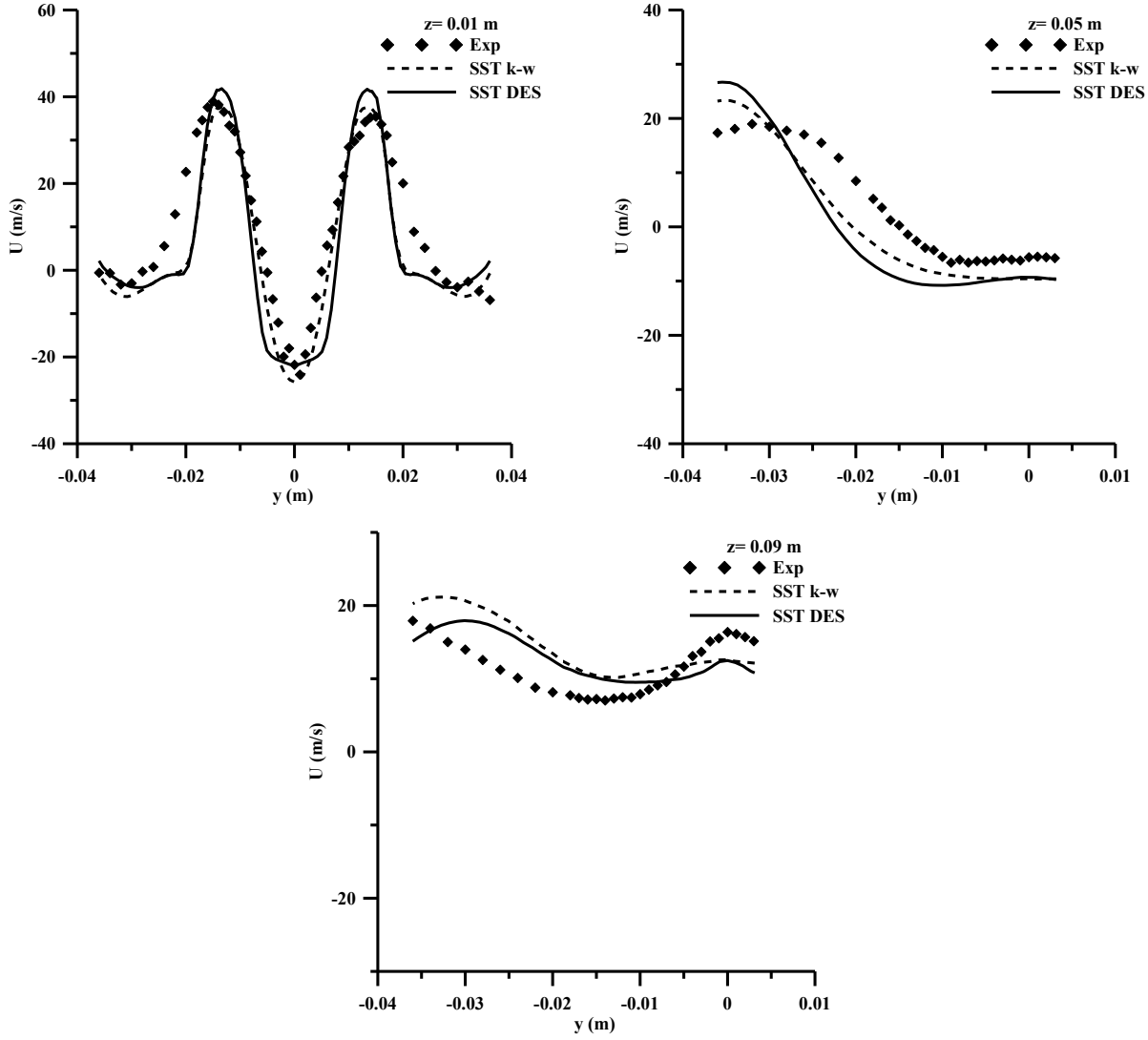

Figure 5. The average axial velocity at the three radial lines: z = 0.01 m, z = 0.05 m and z = 0.09 m.

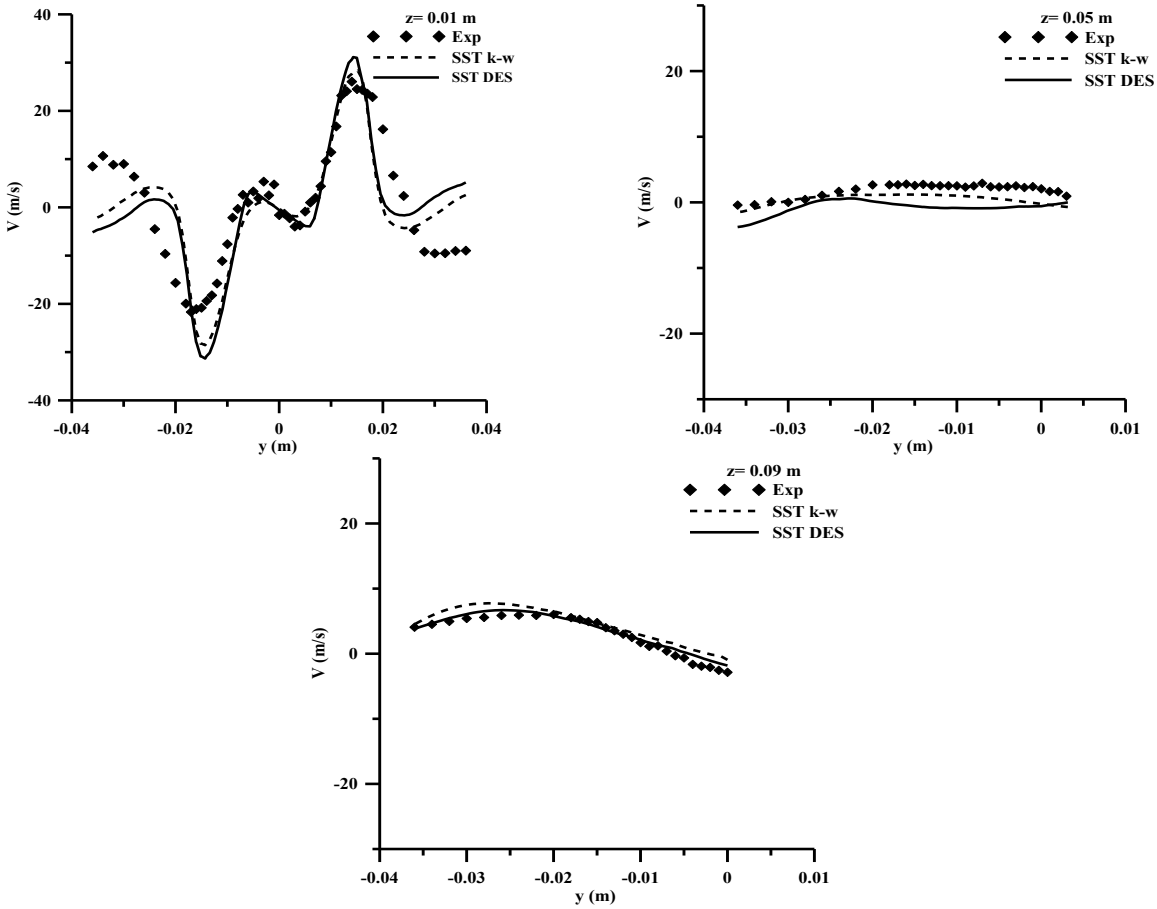

Figure 6. The average radial velocity at the three radial lines: z = 0.01 m, z = 0.05 m and z = 0.09 m.

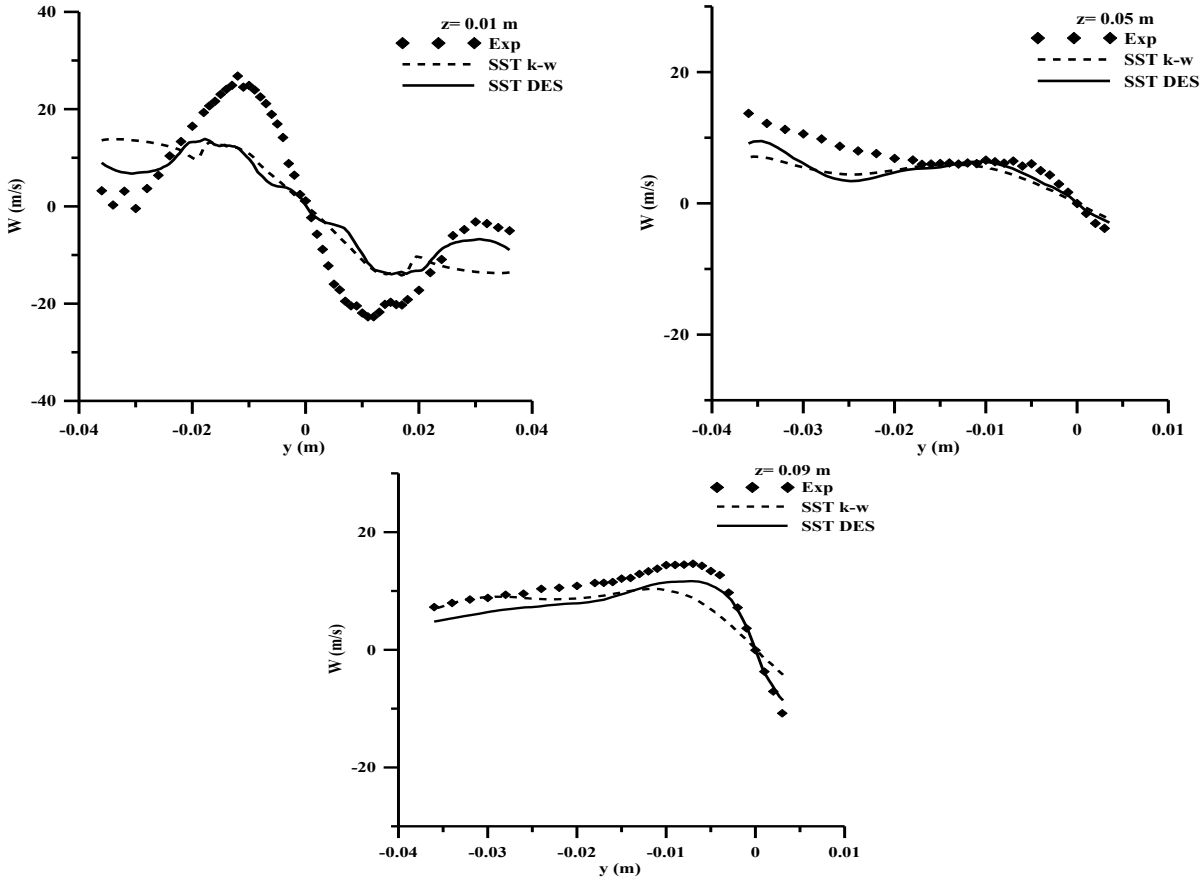

Figure 7. The average tangential velocity at the three radial lines: z = 0.01 m, z = 0.05 m and z = 0.09 m.

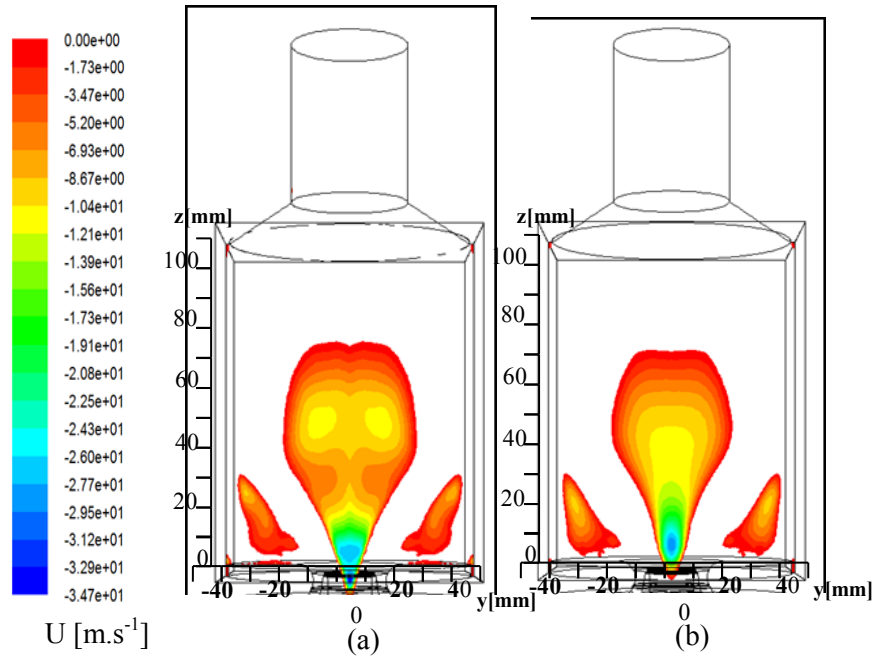

Figure 8. Contours of negative average axial velocity: (a) SST-DES and (b) SST k-ω models.

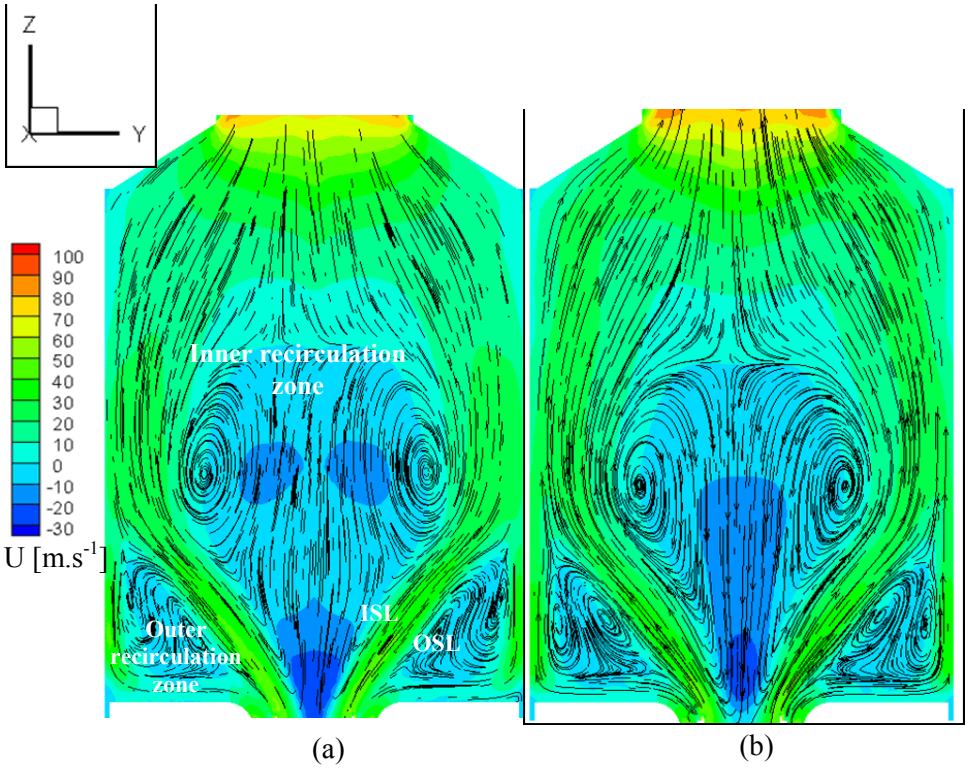

Figure 9. Time averaged streamlines and axial velocity contours in the center plane of the combustor calculated using the (a) SST-DES and (b) SST k-ω models.

Figure 10 compares time averaged temperature profiles obtained numerically, using the SST-DES and SST k-ω models, at the three radial lines: z= 0.01 m, z = 0.05 m and z= 0.09 m shown in Figure 1 with the experimental data. The general features of the measured temperature profiles are reasonably well predicted near the central axis for the three positions. At z = 0.01 m the simulations using both SST-DES and SST k-ω models correctly reproduce the temperature at the inner recirculation zone (-0.01 m ≤ y ≤ 0.01 m) with an error not exceeding 6% at the central axis. However, the temperature is overestimated especially at the outer recirculation zone. This discrepancy can be due to the combustion model used as well as the fact that radiation effects were not taken into account.

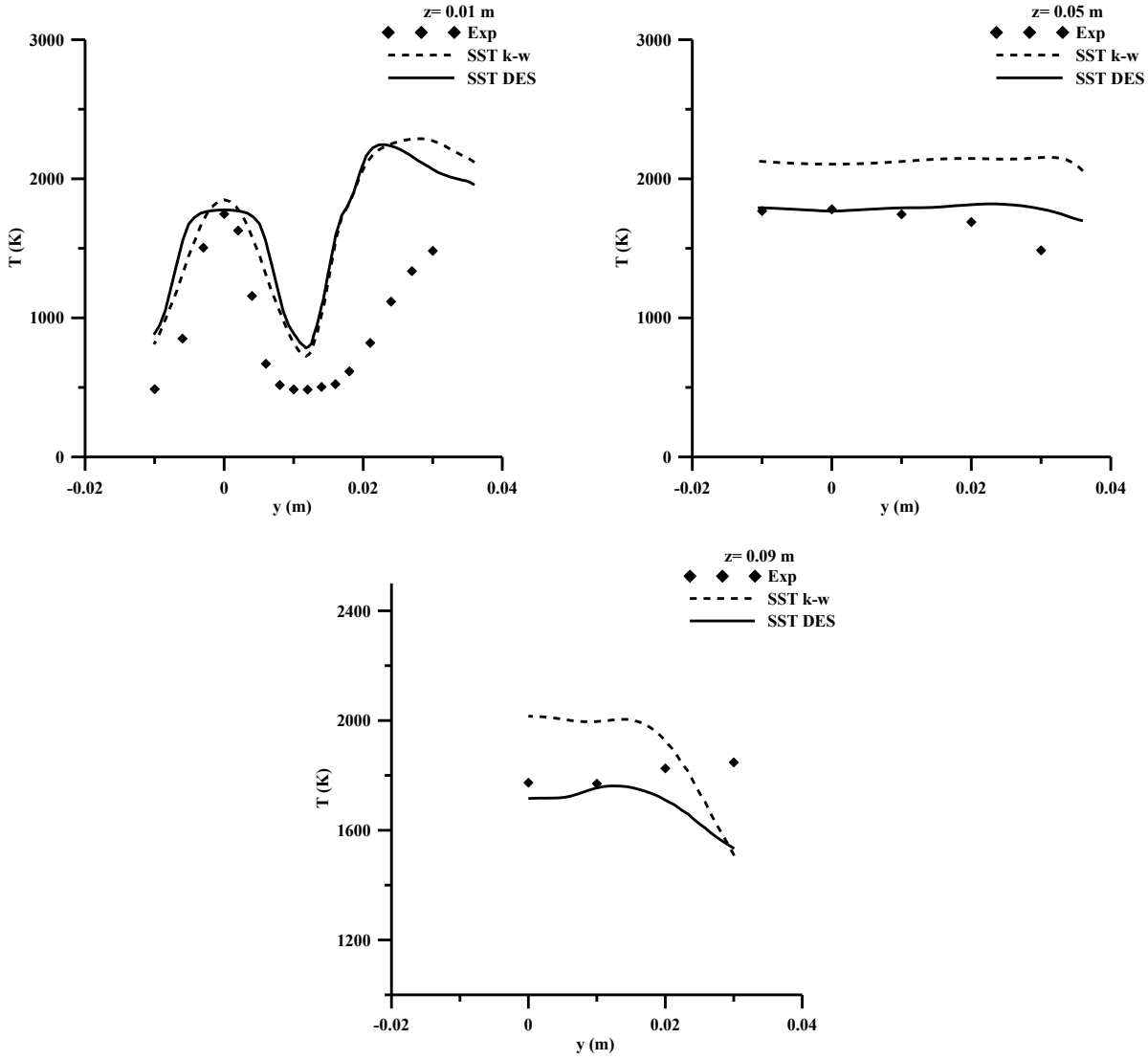

Figure 10. The average temperature at the three radial lines: z = 0.01 m, z = 0.05 m and z = 0.09 m.

At z = 0.05 m and z = 0.09 m the radial profiles of temperature are better predicted and the agreement between experimental data and the numerical results of the SST-DES model are more satisfactory. In fact, numerical predictions of the SST-DES model match the experimental measurement quite well with errors less than 7 % at the inner recirculation zone (-0.01 m ≤ y ≤ 0.01 m) and less than 16% at the outer recirculation zone. However, the SST k-ω model greatly overestimates the temperature at those locations with an error reaching 20 % at the inner recirculation zone and 37% at the outer recirculation zone.

This discrepancy between the numerical results of the two models can be explained by the fact the quality of the predictions using the Eddy Dissipation combustion model is highly dependent on the performance of the turbulence model used due to the dependence of the fuel dissipation rate on the turbulence time scale. For this reason, the SST-DES model outperforms the SST k-ω model, which cannot handle the details of unsteady flow and turbulence–combustion interactions since it suppresses unsteady turbulent fluctuations by time averaging.

Figure 11 gives the contours of time averaged temperature calculated using the SST-DES (Figure 11a) and the SST k-ω (Figure 11b) models in the central vertical plane (x = 0 m) of the combustor. As expected the predicted temperature using the SST k-ω model are larger than the results of the SST-DES model especially in the inner recirculation zone. The predicted profile of temperature using the SST-DES model shows that highest temperatures are located close to the nozzle exit near the methane injections. It can be seen that the temperature in the corner recirculation zone is higher compared to the inner recirculation zone. The high temperatures in this zone indicate the presence of a large fraction of already burned gases. The temperature in the inner recirculation zone reaches a value of 1800 K. The inner

recirculation zone constitutes a well-mixed region that serves to transport heat to the fresh combustible jets of air and methane. It is noticed that hot gases reach even the inside the central air nozzle, allowing the preheating of the incoming air.

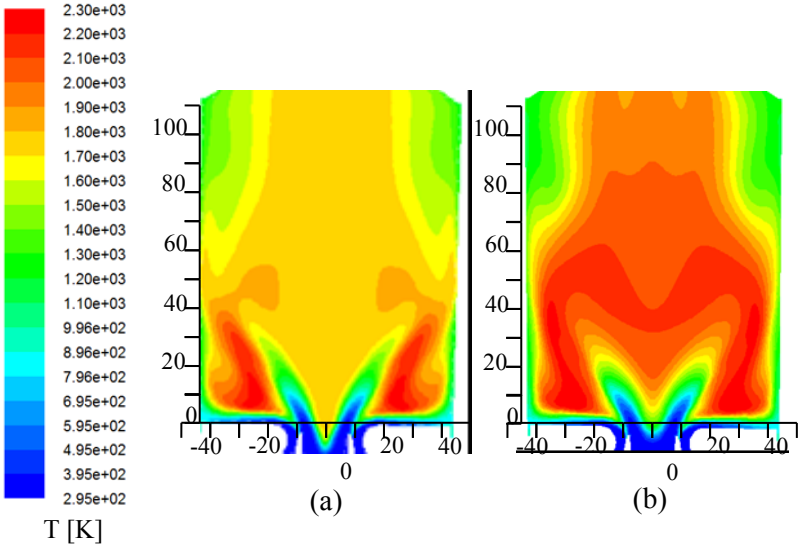

Figure 11. Contours of the average temperature in a central cross section of the combustion chamber: a) SST-DES and b) SST k-ω models.

Figures 12 and 13 compare time averaged CH_4 and H_2O mass fractions profiles obtained numerically, using the SST-DES and SST k-ω turbulence models, at the radial line: z = 0.01 m with the experimental data.

Figure 12 shows that the general trend of CH_4 mass fraction average profile is well captured by the two used models, however the peak value is overestimated by about 40 % and shifted compared to the experimental data.

Concerning the H_2O mass fraction shown in Figure 13, the general features of the measured profile is very well predicted near the central axis with an error not exceeding 11%. The simulations using both SST-DES and SST k-ω models correctly reproduce H_2O mass fraction at the inner recirculation zone (-0.01 m ≤ y ≤ 0.01 m). However, this latter is overestimated especially in the outer recirculation zone. This discrepancy can be due to the combustion model used as well as the reduced chemical scheme used.

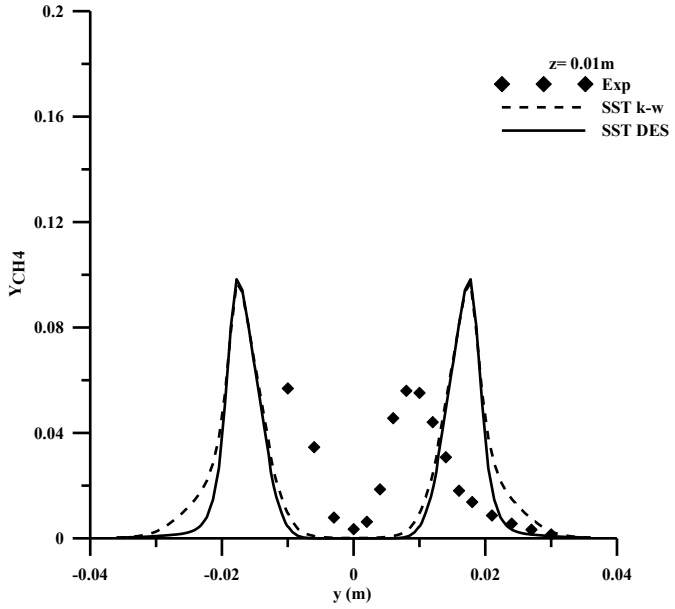

Figure 12. The average CH_4 mass fraction at the radial line: z = 0.01 m.

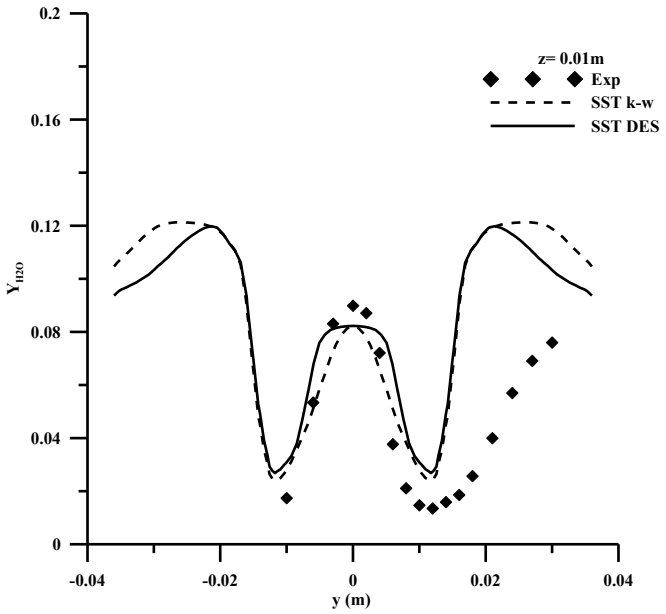

Figure 13. The average H_2O mass fraction at the radial line: z = 0.01 m.

4.2 Unsteady flow fields

We first propose to show, in which regions the flow is resolved by RANS and LES methods in the simulations using the SST-DES turbulence model.

Figure 14 presents the contours of relative length scale defined by:

$$L_{t,R} = L_{t,SST} - L_{t,LES} \tag{21}$$

All of the zones inside the domain in which $L_{t,R} > 0$ belong to the LES region. However, all of the zones inside the domain in which $L_{t,R} < 0$ belong to the RANS region. As shown in Figure 14 the SST k-ω model is used in the boundary layers and a subgrid model in the core regions.

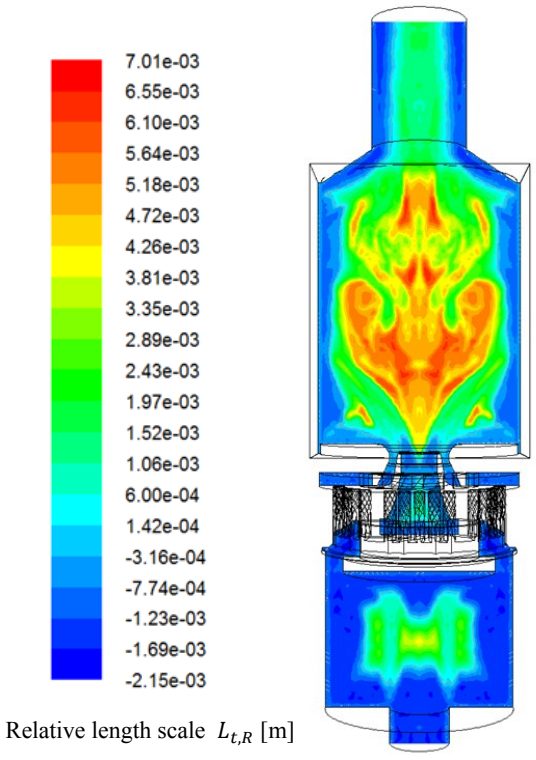

Figure 14. Contours of relative length scale (SST-DES model).

Figures 15, 16, and 17 show comparisons of measured and computed Root Mean Square (RMS) fluctuations of axial, radial, and tangential velocities respectively. The predictions of RMS velocity fluctuations have been obtained using the SST-DES model. It can be noticed that the SST-DES computations predict well the profile shapes. However, it can be seen that the SST-DES results under predict the centerline region values at z = 0.01 m for the three velocities. The agreement between the calculations and measurements for the RMS fluctuations of the radial velocity is better at the two other axial locations (z = 0.05 m and z = 0.09 m).

Figure 18 and Figure 19 show the instantaneous negative axial velocity and temperature fields in the vertical section (x = 0 mm) of the combustion chamber, calculated using the SST-DES model, at t = 0.92 s, t = 0.93 s, t = 0.94 s, and t = 0.95 s. It can be seen that the instantaneous flow fields contain distinctive features that are not present in the average flow fields discussed in section 3.1 (Figure 9 and Figure 11). As expected the flow is highly unsteady. The size, the shape as well as the position of the inner and outer recirculation zones are instationnary. It can be clearly noticed that the sizes of the inner and outer recirculation zones have a strong influence on the shape and the position of the flame. In fact, the inner recirculation zone is more extended in the radial direction at t = 0.93s and results to a flame closer to the chamber walls. In the other hand, the inner recirculation zone is less extended in the radial direction at t = 0.92s, hence, it can be seen that the flame recedes from the chamber walls. Figure 18 and Figure 19 also put in evidence that the size of the corner recirculation zone influences the shape and the position of the flame. In fact, it can be noticed that when the corner recirculation zone is less extended and weaker the flame recedes from the chamber walls (t = 0.95 s) and vice versa (t = 0.93 s and t = 0.94 s). It is noted that further unsteady recirculation zones are observed inside the plenum.

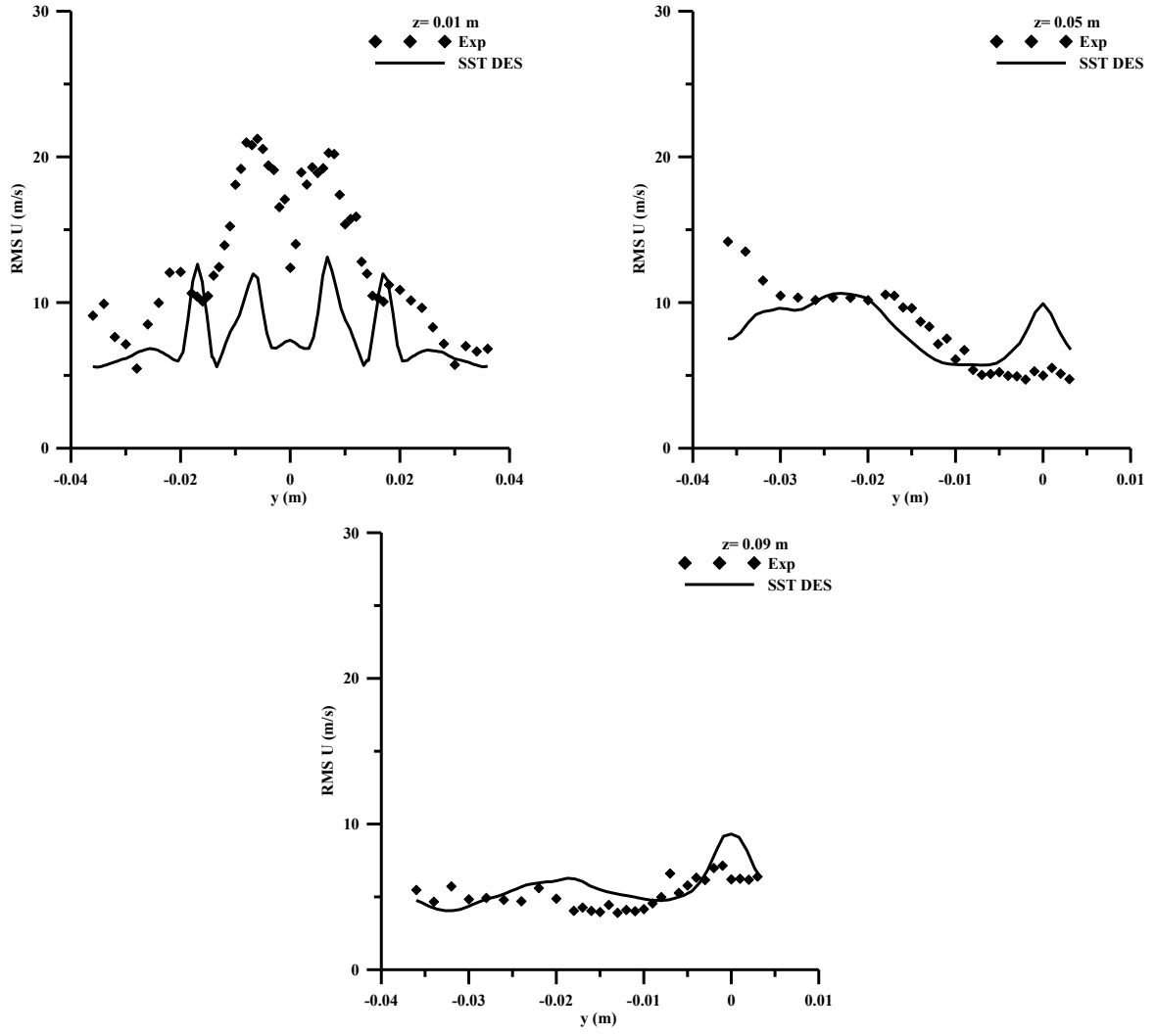

Figure 15. Root Mean Square (RMS) fluctuations of the axial velocity obtained using the SST-DES model.

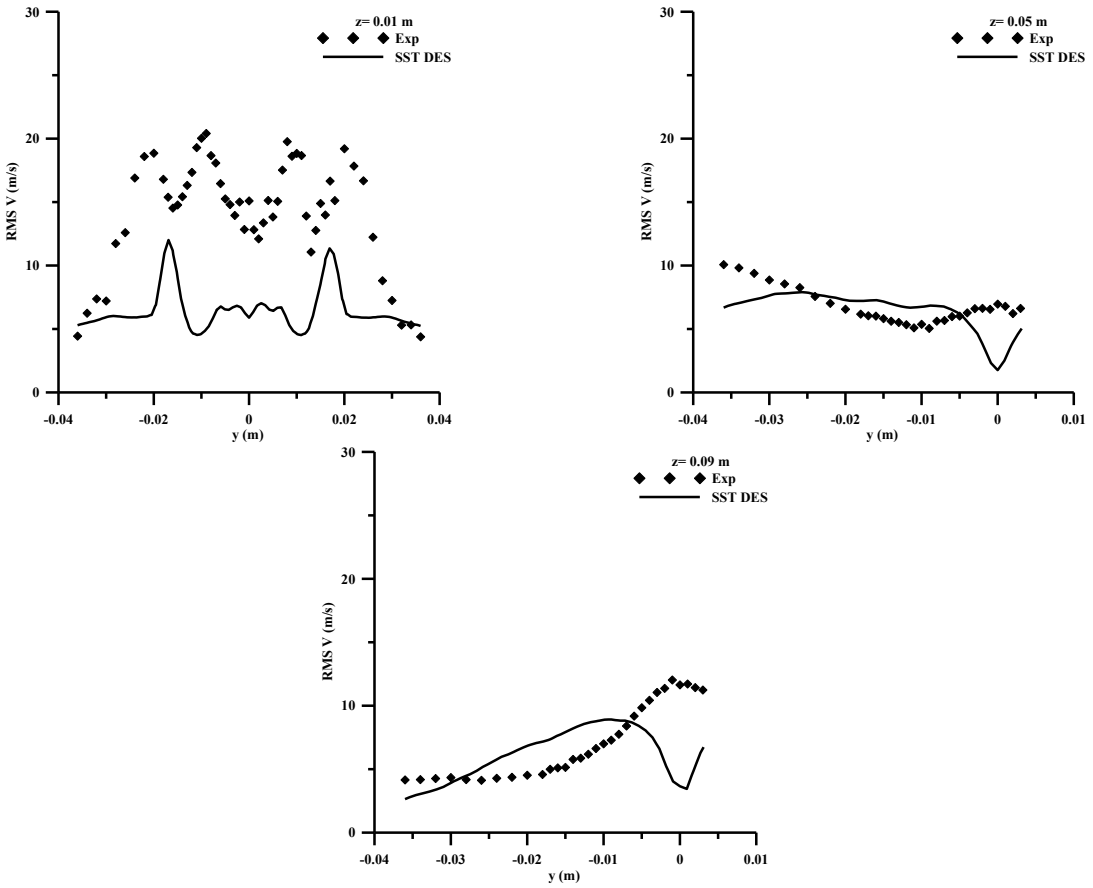

Figure 16. Root Mean Square (RMS) fluctuations of the radial velocity obtained using the SST-DES model.

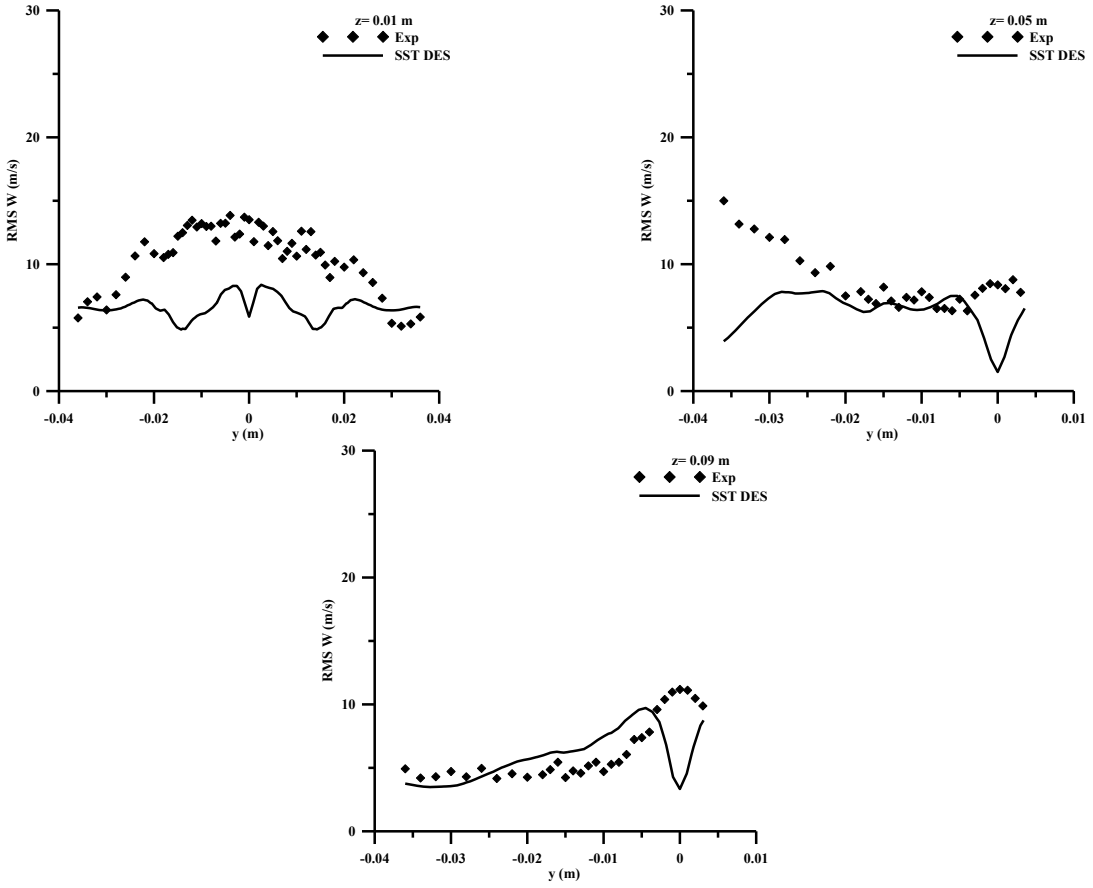

Figure 17. Root Mean Square (RMS) fluctuations of the tangential velocity obtained using the SST-DES model.

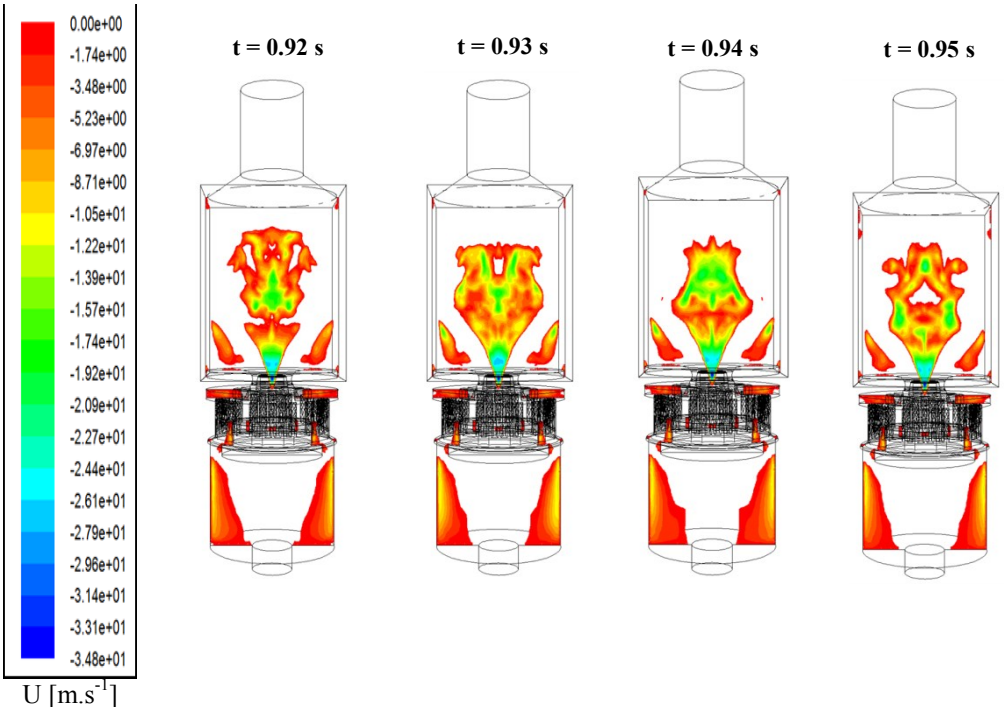

Figure 18. Contours of the instantaneous negative axial velocity in a central cross section of the combustion chamber, calculated using the SST-DES model, at t = 0.92 s, t = 0.93 s, t = 0.94 s and t = 0.95 s.

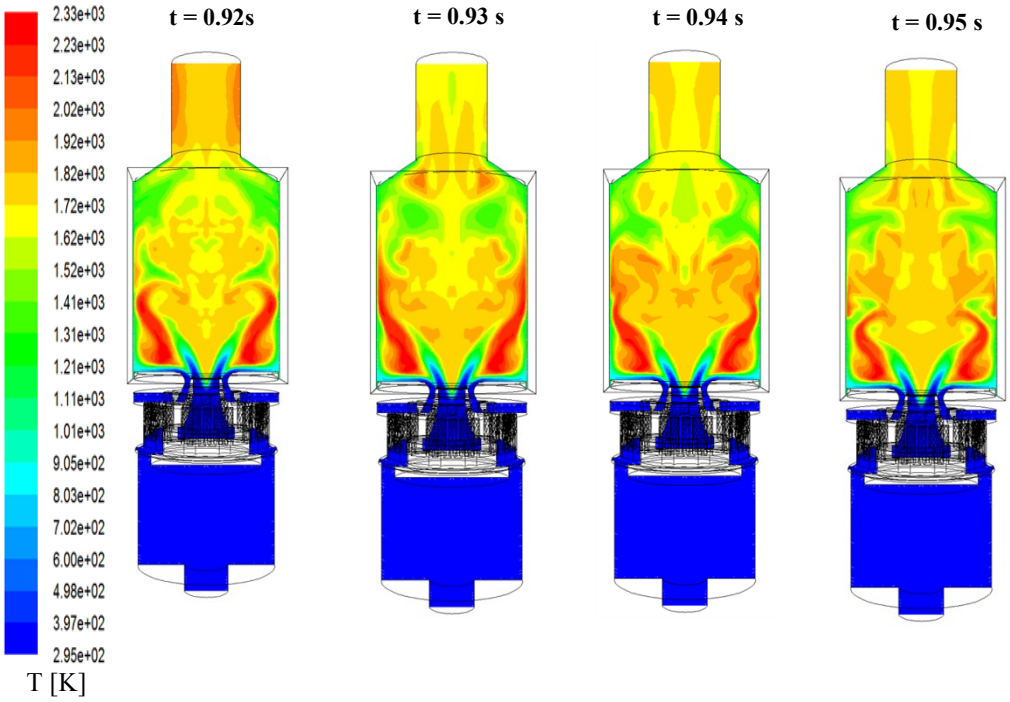

Figure 19. Contours of the instantaneous temperature in a central cross section of the combustion chamber, calculated using the SST-DES model, at t = 0.92 s, t = 0.93 s, t = 0.94 s and t = 0.95 s.

To further explore the dynamics of the flow, we examine the instantaneous streamlines in the vertical central section (x = 0 m) illustrated in Figure 20.

The instantaneous streamline plots obtained using the SST-DES turbulence model (Figure 20a) show clearly the existence of many vortex structures in the outer and inner recirculation zones and especially close to the inner and outer shear layers. These phenomena are not visible in the time-averaged SST-DES (Figure 9) and in the instantaneous streamlines plots predicted using the SST k-ω model (Figure 20b).

It can be seen that the flow is very complicated and include energetic vortex structures of different sizes. In fact, in addition to the two large scale vortices located in the center of the chamber, there are numerous small-scale vortices found on the inner and outer shear layer of the incoming flow as well as in the vicinity of the combustor axis. The resolution of such flow phenomena might be decisive for the quality of a simulation of the turbulent combustion processes. For this reason, better predictions of the thermal field are obtained in this study using the SST-DES model compared to the SST k-ω model (section 3.1).

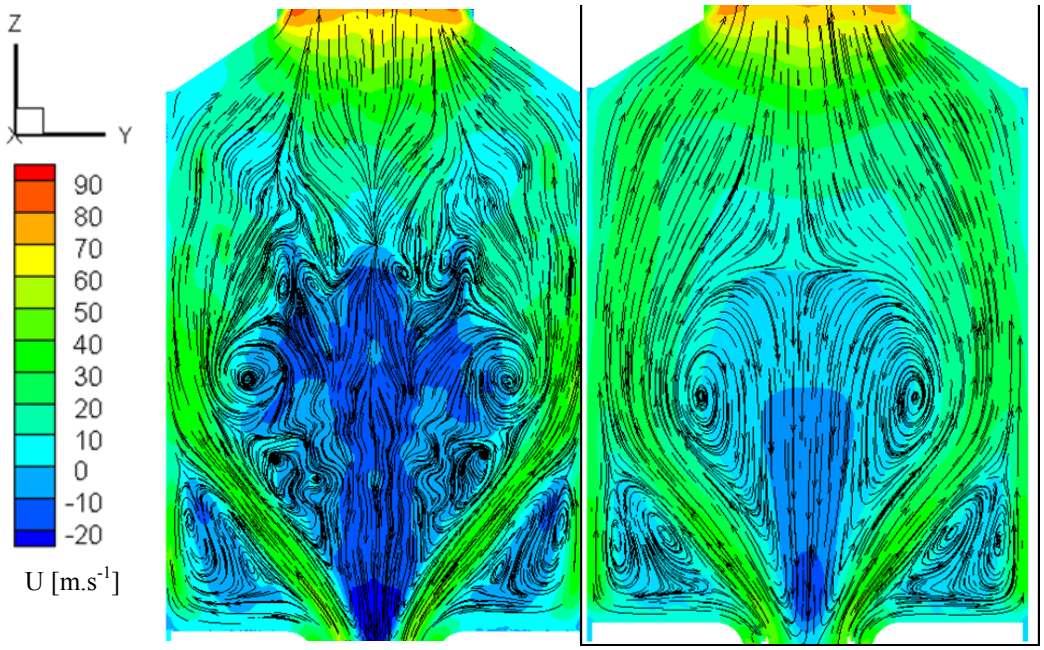

Figure 20. The instantaneous streamlines in a central cross section of the combustion chamber: (a) SST-DES and (b) SST k-ω models.

5. Conclusion

The ability of the hybrid RANS/LES Detached Eddy Simulation turbulence model to correctly predict the reacting flow within a swirl stabilized GTMC have been worked out. The three dimensional calculations of a swirled gas turbine model combustor using DES and URANS methods and the commercial solver ANSYS-FLUENT were presented. The computational domain matches identically the complex laboratory configuration of a 35 kW burner, developed by the German Aerospace Center (DLR), fed with methane and characterized by a 0.65 overall equivalence ratio. On the whole, a satisfactory agreement between the numerical results and the available experimental data of the time averaged flow was found using the two methods. However, the SST k-ω turbulence model over predicts the temperature compared to SST-DES model results and experimental data. Moreover, the SST-DES model provides much detailed information about instantaneous flow patterns than the SST k-ω turbulence model results.

In fact, numerical results of the time averaged flow fields of both SST-DES and SST k-ω turbulence models showed a large central recirculation zone and a corner recirculation zone which represents a typical result of confined swirl flames. However, the SST-DES model results revealed from the obtained instantaneous flow fields that the size, the shape as well as the position of the central and corner recirculation zones are unsteady. Average streamlines plots showed that the inner recirculation zone is formed by two counter rotating vortex pair, while instantaneous streamlines plots showed clearly the existence of numerous small unsteady vortex structures in that zone.

Acknowledgments

The authors thank Dr Wolfgang Meier from the Deutsches Zentrum für Luft- und Raumfahrt DLR (Institute of Combustion Technology) for providing the experimental research data sets of the swirling CH_4/air flames of the swirled gas turbine model combustor acquired at the Institute.

References

[1] Eldrainy Y A, Saqr K M, Aly H S, Tholudin M L, Mohd Jaafar N M. Large eddy simulation and preliminary modeling of the flow downstream a variable geometry swirler for gas turbine combustors. Int Commun Heat Mass 2011; 38: 1104-9.

[2] Shengli W, Feihu W, Xianyin L, Xin L, Kunpeng J. Numerical analysis on the effect of swirl ratios on swirl chamber combustion system of DI diesel engines. Energy Convers Manage 2013; 75: 184–190.

[3] Yang W, Zhang J. Simulation of swirling turbulent combustion in the TECFLAM combustor. Comput Chem Eng 2008; 32: 2280–9.

[4] Frassoldati A, Frigerio S, Colombo E, Inzolib F, FaravelliT, Determination of NOx emissions from strong swirling confined flames with an integrated CFD-based procedure. Chem Eng Sci 2005; 60: 2851–69.

[5] Roux S, Lartigue G, Poinsot T, Meier U, Bérat C, Studies of mean and unsteady flow in a swirled combustor using experiments, acoustic analysis, and large eddy simulations, Combust Flame 2005;141:40-54.

[6] Vengadesan S, Nithiarasu P. Hybrid LES – Review and assessment. Sadhana 2007; 32: 501-11.

[7] Zhou L X, Hu L Y, Wang F. Large-eddy simulation of turbulent combustion using different combustion models. Fuel 2008; 87: 3123-31.

[8] Galpin J, Naudin A, Vervisch L, Angelberger C, Colin O, Domingo P. Large-eddy simulation of a fuel-lean premixed turbulent swirl-burner. Combust Flame 2008;155: 247–66.

[9] Franzelli B, Riber E, Gicquel L Y M, Poinsot T. Large Eddy Simulation of combustion instabilities in a lean partially premixed swirled flame. Combust Flame 2012; 159: 621-37.

[10] Bunge U, Mockett C, Thiele F. Guidelines for implementing Detached-Eddy Simulation using different models. Aerosp Sci Technol 2007; 11: 376–85.

[11] Spalart P R., Jou W H., Strelets M, Allmaras S R. Comments on the feasibility of LES for wings, and on a hybrid RANS/LES approach. In: Liu C, Liu Z, editors. Advances in DNS/LES. First AFOSR International Conference on DNS/LES; 1997 August 4–8, Ruston, LA, Greyden Press, Columbus, OH.

[12] Mockett C., Fuchs M., Thiele F., Progress in DES for wall-modelled LES of complex internal flows, Comput Fluids 2012; 6: 44–55.

[13] P.R Spalart, Strategies for turbulence modelling and simulations, International Journal of Heat and Fluid Flow Int J Heat Fluid Fl 2000; 21: 252–263.

[14] You Y, Luedeke H, Hannemann K. Injection and mixing in a scramjet combustor: DES and RANS studies. P Combust Inst 2013; 34: 2083–92.

[15] Gant Simon E. Reliability Issues of LES-Related Approaches in an Industrial Context. Flow Turbul Combust 2010; 84: 325-335.

[16] Zhou H, Cen K, Fan J. Detached eddy simulation of particle dispersion in a gas-solid two-phase fuel rich/lean burner flow. Fuel 2005; 84: 723-31.

[17] Walters D K, Bhushan S, Alam M F, Thompson D S. Investigation of a Dynamic Hybrid RANS/LES Modelling Methodology for Finite-Volume CFD Simulations. Flow Turbul Combust 2013; 91: 643-67.

[18] Viswanathan A K, Tafti D K. Detached eddy simulation of turbulent flow and heat transfer in a two-pass internal cooling duct. Int J Heat Fluid Fl 2006; 27: 1–20.

[19] Sentyabov A V, Gavrilov A A, Dekterev A A. Investigation of turbulence model for computation of swirling flows. Thermophys Aeromech 2011; 18: 73-85.

[20] Widenhorn A, Noll B, Stohr M, Aigner M. Numerical Characterization of the Non-Reacting Flow in a Swirled Gas turbine Model Combustor. In: Nagel W E, Kröner D B, Resch M M. High Performance Computing in Science and Engineering `07. Springer Berlin Heidelberg; 2008. p. 431-44.

[21] Widenhorn A, Noll B, Aigner M, Numerical Characterization of the Reacting Flow in a Swirled Gas turbine Model Combustor. In: Nagel W E, Kröner D B, Resch M M. High Performance Computing in Science and Engineering '08. Springer Berlin Heidelberg; 2009. p. 365-380.

[22] Widenhorn A, Noll B ,Aigner M, Numerical Characterization of a Gas Turbine Model Combustor. In: Nagel W E, Kröner D B, Resch M M. High Performance Computing in Science and Engineering'09. Springer Berlin Heidelberg; 2010. p. 179-195.

[23] Menter F R., Egorov Y. A Scale-Adaptive Simulation Model Using Two- Equation Models. AIAA-Paper, 2005-1095/ Menter, F.R., Kuntz, M., Bender, R.: A Scale Adaptive Simulation Model for Turbulent Flow Prediction. AIAA Paper, 2003-0767
[24] Meier W. Duan X R, Weigand P, Reaction zone structures and mixing characteristics of partially premixed swirling CH4/air flames in a gas turbine model combustor, P Combust Inst 2005; 30: 835-42.
[25] Weigand P, Meier W, Duan X R, Giezendanner-Thoben R, Meier U. Laser Diagnostic Study of the Mechanism of a Periodic Combustion Instability in a Gas Turbine Model Combustor. Flow Turbul Combust 2005; 75: 275–92.
[26] Duan X R., Meier W, Weigand P, Lehmann B. Phase-resolved laser Raman scattering and Laser Doppler Velocimetry applied to periodic instabilities in a gas turbine model combustor. Appl. Phys. B 2005; 80:389–96.
[27] Giezendanner R, Weigand P, Duan X R, Meier W, Meier U, Lehmann B et al. Characterization of Thermoacoustic Instabilities in a Gas Turbine Model Combustor by Laser Spectroscopic Measurements. ECM 2003: Proceeding of the European Combustion Meeting 2003. European Combustion Meeting; Orléans, 2003 October 25-8.
[28] Duan X R, Weigand P, Meier W, Keck O, Stricker W, Aigner M, Lehmann B. Experimental investigations and laser based validation measurements in a gas turbine model combustor. Prog Comput Fluid Dy 2004; 4: 175–82.
[29] Weigand P, Meier W, Duan X R, Stricker W, Aigner M. Investigations of swirl flames in a gas turbine model combustor I. Flow field, structures, temperature, and species distributions. Combust Flame 2006; 144: 205-24.
[30] Meier W, Duan X R, Weigand P. Investigations of swirl flames in a gas turbine model combustor II. Turbulence–chemistry interactions. Combust Flame 2006; 144: 225-236.
[31] Mc Bride B J, Gordon S, Reno M A. Coefficient for calculating thermodynamic and transport properties of individual species, NASA; 1993. Report TM-4513.
[32] Menter F R. Two-equation turbulence-models for engineering applications. AIAA J 1994; 32 (8):1598–1605.
[33] Wilcox D C. Reassessment of the scale-determining equation for advanced turbulence models. AIAA J 1988; 26 (11): 1299-1310.
[34] ANSYS FLUENT Theory Guide, ANSYS, Inc., Release 14.0, 2011.
[35] Squires K D. Detached-Eddy Simulation: Current Status And Perspectives. In: Friedrich R, Geurts B J, Métais O. Direct and Large-Eddy Simulation. VERCOFTAC Series. Springer Netherlands; 2004; 9; p. 465-80.
[36] Magnussen B F, Hjertager B H. On mathematical models of turbulent combustion with special emphasis on soot formation and combustion. In: 16th Symp (int) on combustion, The Combustion Institute;1976; 16: 719–29.
[37] Saqr K M, Aly H S, Sies M M, Abdul Wahid M. Implementation of the eddy dissipation model of turbulent non-premixed combustion in Open FOAM. Int Commun Heat Mass 2011; 38: 363-67.
[38] Tsioumanis N, Brammer JG, Hubert J. Flow processes in a radiant tube burner: Combusting flow. Energy Convers Manage 2011; 52: 2667–75.
[39] Yılmaz I, Tastan M, Ilbas M, Tarhan C. Effect of turbulence and radiation models on combustion characteristicsin propane–hydrogen diffusion flames. Energy Convers Manage 2013; 72: 179-86.
[40] Hosseini S E, Bagheri G, Abdul Wahid M. Numerical investigation of biogas flameless combustion. Energy Convers Manage 2014; 81: 41-50.
[41] Meier W, Duan X R, Weigand P. Reaction zone structures and mixing characteristics of partially premixed swirling CH4/air flames in a gas turbine model combustor. P Combust Inst 2005; 30: 835-42.
[42] Hirsch C. Numerical computation of internal and external flows. Fundamentals of numerical discretization. vol. 1. Wiley & Sons; 1994.
[43] Lucca-Negro O, O'Doherty T. Vortex breakdown: a review, Prog Energ Combust 2001; 27: 431-81.

